Optimization and Engineering
https://doi.org/10.1007/s11081-022-09728-1

RESEARCH ARTICLE

Current and voltage control system designs with EKF-based state-of-charge estimator for the purpose of $LiFePO_4$ battery cell charging

Danijel Pavković[1] · Antun Premec[1] · Matija Krznar[1] · Mihael Cipek[1]

Received: 24 November 2021 / Revised: 16 March 2022 / Accepted: 22 April 2022

Abstract

This paper presents two designs of constant-current/constant voltage battery charging control systems in the form of a cascade control system arrangement with the superimposed proportional-integral (PI) controller commanding the battery charging current reference to the inner PI controller-based current control loop. The superimposed control level can be realized as: (i) battery terminal voltage limiting control loop, or (ii) battery state-of-charge (SoC) control loop based on SoC estimation using an extended Kalman filter, which augments the battery terminal voltage control loop in a straightforward way. The design of such modular control system is based on the suitable control-oriented model of the battery charging process and utilization of damping optimum criterion. The effectiveness of the proposed battery charging control system has been verified by means of simulations using the readily available experimentally-obtained model of a lithium-iron-phosphate ($LiFePO_4$) battery cell, which has shown notable potential for charging process speedup when traditional battery voltage limiting control is augmented with the SoC control loop.

Keywords Lithium-iron-phosphate battery cell · Constant-current/constant voltage charging · Cascade control · State-of-charge estimation · Extended Kalman filter · Simulations

✉ Mihael Cipek
mihael.cipek@fsb.hr

Danijel Pavković
danijel.pavkovic@fsb.hr

Antun Premec
antun.premec@gmail.com

Matija Krznar
matija.krznar@fsb.hr

[1] Faculty of Mechanical Engineering and Naval Architecture, University of Zagreb, Ivana Lučića 5, 10000 Zagreb, Croatia

Published online: 10 June 2022

Abbreviations

Ah	Ampere-hour (charge capacity unit)
ANN	Artificial neural network
CCCV	Constant-current/constant voltage (charging regime)
CCCV-VL	CCCV charging control with battery voltage limiting
CCCV-SoC	CCCV charging control with SoC reference and battery voltage limiting
DC	Direct current
DC/DC	Direct current to direct current (power conversion)
DP	Dynamic Programming
EKF	Extended Kalman filter
$LiFePO_4$	Lithium-iron-phosphate (battery cell technology)
MCC	Multi-level constant-current (charging technique)
MPC	Model predictive control
OCV	Open-circuit voltage
PI	Proportional-integral (controller)
PWM	Pulse-width modulation
SoC	State-of-charge
SoH	State-of-health
UKF	Unscented Kalman filter

Variables

d	Buck converter pulse-width modulation (PWM) duty cycle
e	State-space model output (measurement) noise
e_{lim}	Voltage limiting PI controller control error input
$\mathbf{F}$, $\mathbf{G}$	State-space model system matrix and input matrix
$\mathbf{h}$	State-space model nonlinear output function
$\mathbf{H}$	Output model Jacobian $\partial\mathbf{h}/\partial\mathbf{x}$
i_b, i_{bm}, i_{bR}	Battery current, battery current measurement and battery current reference
i_{blim}	Battery current limiting command
i_r, i_{rL}	Active rectifier output current and DC bus load current
I_b, $\overline{u}_b$	Average battery current and average battery terminal voltage
k	Sampling step
$\mathbf{K}$, $\mathbf{P}$	Kalman filter gain matrix and prediction error covariance matrix estimate
$\mathbf{Q}$	Stochastic state-space model state disturbance covariance matrix
Q_p, r_m	Parameter variance and measurement variance in parameter estimator design
P, K	Parameter estimator error covariance and measurement correction gain
I_{max}	Battery current limit
q^{-1}	Unit sample delay operator
r	Measurement (output) noise variance in state estimator design
$\hat{R}_b$, $\hat{R}_p$	Estimated values of battery series resistance and polarization resistance

s	Laplace operator
u_c, u_{cR}	Buck converter output voltage and its target value
u_{dc}, u_{dcm}	DC bus voltage and its measurement value
u_{blim}	Battery terminal voltage limit value
U_{oc}	Battery open-circuit voltage
U_{max}	Buck converter output voltage limit
u_b, u_{bm}	Battery terminal voltage and terminal voltage measurement
u_p, u_{pe}	Battery polarization voltage and polarization voltage estimate
$\overline{u}_p$	Battery polarization voltage average value
$\mathbf{x}$	State variable vector
$\Delta\xi$	EKF-based estimator SoC estimation error
Δi_b, Δu_b	Battery current and terminal voltage variation (numerical difference)
ε	Extended Kalman filter prediction error
ε_b, ε_p, ε_Q	Series and polarization resistance error, and charge capacity error
$\boldsymbol{\nu}$	Stochastic state-space model state disturbance vector
ξ, ξ_e, ξ_R	Battery state-of-charge (SoC), SoC estimate and SoC target, respectively
$\boldsymbol{\Omega}$	Stochastic state-space model state disturbance scaling matrix

Parameters

a	Polarization lag-related parameter of discrete-time battery model
C_{in}	Input capacitance of buck DC/DC converter
D_2, …, D_n	Damping optimum characteristic ratios
D_{2i}, D_{3i}	Damping optimum characteristic ratios in current PI controller design
D_{2l}, D_{3l}	Damping optimum characteristic ratios in voltage PI controller design
$D_{2\zeta}$, $D_{3\zeta}$	Damping optimum characteristic ratios in SoC PI controller design
K_{ci}, $K_{cl,}$ $K_{c\xi}$	Proportional gains of PI controllers for current, voltage and SoC
T_{ci}, $T_{cl,}$ $T_{c\xi}$	Integral time constants of PI controllers for current, voltage and SoC
Q_b, R_b	Battery charge capacity and internal resistance
R_p, C_p	Battery polarization resistance and capacitance, respectively
R_c, L_c	Equivalent resistance and inductance of inductor
T_e	Equivalent closed-loop time constant (damping optimum criterion)
T_{ei}, T_{el}	Equivalent time constants in current and voltage control system designs
$T_{e\xi}$	Equivalent time constant in SoC control system design
T_{fm}, T_{pc}	Current and voltage sensor time constant and power converter equivalent lag
$T_{\Sigma i}$, $T_{\Sigma u}$	Parasitic time constants in current and voltage/SoC PI controller designs
ϑ_b	Battery temperature
τ_p	Battery polarization voltage time constant
ζ	Damping ratio

Symbols

$\wedge$	Estimated value (state variable)
$-$	Average value

D	Freewheeling diode within buck converter
Q	MOSFET switch within buck converter

1 Introduction

The analysis carried out by McCollum et al. (2014) has indicated that about 20% of the world production of fossil fuels is consumed by the transportation sector, which subsequently results in a proportionally large share of its greenhouse gases emissions. In order to increase its energy efficiency and make it more environmentally friendly and less dependent on oil reserves, transportation sector electrification has been proposed by Buzzonii and Pede (2012), along with its integration within the smart electricity grid paradigm (Deur et al. 2015). This type of transport and energy sector integration usually entails the specific requirements of electrical vehicle fleets in terms of fleet electrification level and charging infrastructure costs and passenger capacity (Chinese et al. 2021), in particular the electric vehicle battery status during charging and discharging needs to be carefully monitored in order to ensure its long service life (Goodall et al. 2019). Optimization of vehicle operating regime-related battery state-of-charge (SoC) profiles and their usefulness for immediate charging is discussed by Aziz et al. (2016). This is further illustrated by Soldo et al. (2021) for the case plug-in hybrid electric city bus fleet. Within such smart grid integration utilization of sophisticated energy management strategies is needed to achieve optimal battery energy storage utilization (Scioletti et al. 2017). Besides the road transport, battery energy storage technologies are also making inroads into the railway transportation sector with battery-hybridized locomotives (Cipek et al. 2019) and battery-electric locomotives (Cipek et al. 2021), both offering distinct advantages over the conventional freight haul, but may require wayside charging in order to maintain optimal battery SoC profiles (Ahmad et al. 2021). The need for effective and timely battery charging in these applications mandates the use of suitable charging control strategies.

In battery charging applications, the so-called constant-current constant-voltage (CCCV) charging technique (Wai and Jhung 2012) is usually preferred when recharging the battery from the discharged state (Hussein and Batarseh 2011), while pulse charging (James et al. 2006) and trickle charging approaches (Hussein and Batarseh 2011) are usually reserved for maintaining the battery charge once it has been fully charged (so-called float charging). The main advantage of the CCCV approach is that the charging current and battery terminal voltage are effectively limited by means of respective battery controllers, thus reducing battery thermal stresses and preventing battery over-voltages, which would otherwise result in accelerated aging and possible cell breakdown. The battery current and voltage controllers can either be switched between depending on the battery terminal voltage conditions (Chen and Rincón-Mora 2006) or used within the so-called cascade control system arrangement as shown by Pavković et al. (2014). In the latter case, the current reference has been commanded by the superimposed battery terminal voltage controller, whose target value corresponds to the final battery voltage at the fully charged state. Thus, the charging control system can easily accommodate for

different battery chemistries characterized by different charging currents and final (fully charged) battery terminal voltage values. In order to facilitate effective current and voltage control during charging, different controller types have been proposed. Hsieh et al. (2001) have proposed a fuzzy logic-based controller which showed clear advantages over the conventional (CCCV) charging framework in terms of charging speed, whereas model predictive control (MPC) has been proposed by Zou et al. (2017) and Zou et al. (2018) to explicitly account for voltage and temperature constraints during charging, thus reducing the battery stresses which would otherwise negatively affect the battery state-of-health (SoH). Similar study has been conducted by Jiang et al. (2014), which have optimized the battery power and current profiles with respect to battery thermal effects in order to balance the charging rate and temperature rise. In that sense, dynamic programming (DP) is used by Chen et al. (2015) to formulate a low power-loss battery charging strategy which minimizes the overall heat losses. Alternative battery charging profiles have also been investigated, with Abdel-Monem et al. (2017) showing that the CCCV technique with negative (discharging) current pulses improves the battery SoH and decelerates battery aging-related phenomena. Similarly, Lee et al. (2018) have demonstrated that using a SoC estimator comprising a temperature-compensated model for supervision of the CCCV battery charging strategy has good potential for charging speed improvement when compared to conventional charging strategy by prolonging the constant-current regime without battery overcharging and over-temperature. Rai et al. (2020) have shown that multi-level constant-current (MCC) charging technique combined with least mean squares (LMS) for the estimation of battery open-circuit voltage (OCV) may yield significant speedup of the charging process, assuming that the OCV versus SoC curve is a-priory known. Offline optimization techniques are also used to determine the optimum charging sequence, such as the genetic algorithm-based optimization proposed by Jiang et al. (2021) in combination with OCV estimation to improve the charging performance (charging speed) at low charging rates, and the so-called Taguchi method presented by Vo et al. (2015) to determine the optimal MCC trajectory, which is then used along with a sliding-mode observer to bring the battery SoC to the desired target value. For a more detailed overview of different charging methods, the reader is referred to the work by Lin et al. (2019).

However, during the charging process, batteries typically exhibit notable terminal voltage versus SoC nonlinear behavior, especially near the highly-discharged and the fully-charged state (Szumanowski and Chang 2008), so SoC monitoring is crucial for safe battery operation during battery charging and discharging regimes. Estimation of battery SoC includes a range of techniques, such as such as Coulomb counting, battery OCV estimation Huang and Chow (2021), impedance spectroscopy, different model-based methods comprising a battery model and suitable dynamic estimator, and artificial neural networks (ANNs) (Meng et al. 2018), as well as fuzzy-logic based models (Samadi and Saif 2017), with optimization-based methods (Wei et al. 2021) and data-driven approaches also being considered by Xiong et al. (2018) and How et al. (2019). Nevertheless, SoC estimation techniques using a suitable dynamic state variable estimator of the Kalman filter type (Plett 2004) still predominate in practical applications due to the fact that they can easily combine the readily available battery terminal voltage and current measurements with

the (typically nonlinear) battery internal model representation, ultimately resulting in a systematic approach to battery sensor fusion. Due to the nonlinear nature of the internal battery model used for SoC estimation purposes, an effective SoC estimator needs to be realized in a nonlinear form, utilizing a range of battery models, such as equivalent circuit model (Zhang et al. 2017) or electrochemical model (Afshar et al. 2019) which may also include the battery model parameter temperature dependence (Zhang et al. 2017). The final model choice is typically a trade-off between the model complexity (i.e. its computational efficiency) and precision, with emphasis given on minimization of the number of model parameters while preserving the desired model accuracy (Fotouhi et al. 2018). Among the model-based approaches, the extended Kalman filter (EKF) and the unscented Kalman filter (UKF) being the most commonly used ones, as indicated by Zhang et al. (2017), Afshar et al. (2019) and Wu et al. (2018), along with the particle filtering approaches (Zhang et al. 2019). A comprehensive estimation technique using hidden Markov model for battery load prediction is combined with recursive least squares algorithm for battery model update to determine the remaining available discharge energy under demanding battery load conditions (Lai et al. 2022). A quite detailed overview of battery SoC estimation techniques are given by Wang et al. (2017) and Lai et al. (2018).

Having the aforementioned aspects of battery charging and SoC estimation in mind, the hypothesis of this work is that by utilizing the precise information about the actual battery state-of-charge, a significant improvement in the effectiveness of the charging process can be achieved through adapting the charging control system with respect to the battery operating point. To this end, this paper presents two distinct designs of a cascade control systems for battery charging applications, wherein the inner current control loop featuring a PI feedback controller is commanded by a superimposed controller in the so-called cascade control system arrangement (Schröder 2007). In the presented approaches, the upper-level (superimposed) controller can either be based on battery terminal voltage feedback or battery SoC feedback. In the latter case, the superimposed controller requires precise information about the battery state-of-charge obtained from a suitably-designed EKF-type SoC estimator, while also requiring an additional (auxiliary) controller for preventing battery terminal voltage exceeding safe levels (i.e. for over-voltage protection). In this sense, the conventional CCCV control strategy is easily augmented by a superimposed SoC estimation-based control loop, thus resulting in a modular charging control system design. Both the inner-loop current PI controller and the outer loop voltage/SoC PI controllers within the proposed cascade control system arrangement are designed utilizing the damping optimum criterion (Naslin 1968). The effectiveness of the proposed modular charging control system is verified by means of simulations using a previously developed model of a lithium-iron-phosphate ($LiFePO_4$) cell, with notable reduction in charging process duration obtained in the case of SoC estimation-based control strategy.

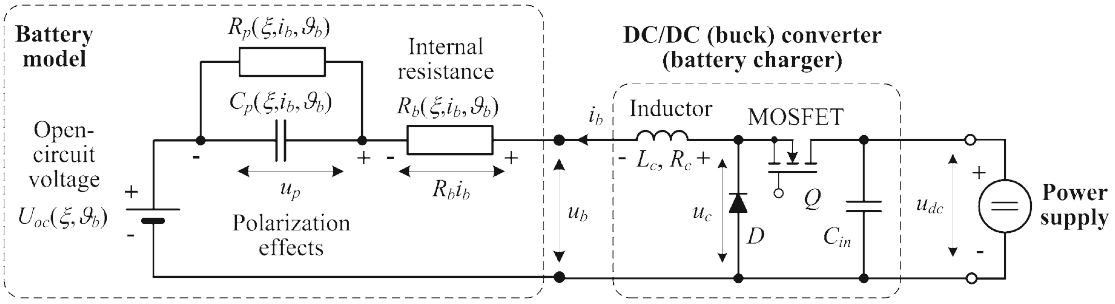

Fig. 1 Principal schematic representation of battery charging system with buck DC/DC converter and battery equivalent electrical circuit model

2 Battery cell and charger circuit dynamic models

This section briefly outlines the dynamic models of lithium-iron-phosphate ($LiFePO_4$) battery cell and buck direct-current to direct current (DC/DC) converter topology suitable for SoC estimator and charging control system design.

2.1 Lithium-iron-phosphate ($LiFePO_4$) battery cell

Figure 1 shows the principal schematic of the basic battery charging system featuring a buck DC/DC converter supplying the charging current to a battery cell depicted by its equivalent electrical circuit model comprising a voltage source signifying the battery open-circuit voltage U_{oc}, electrolyte polarization effects modeled by an equivalent parallel RC circuit (with resistance R_p and capacitance C_p parameters) and an equivalent series resistance R_b (Roscher and Sauer 2011). The above model results in the following voltage u_b versus current i_b relationship in the Laplace s-domain ($\tau_p = R_p C_p$ is the polarization dynamics equivalent time constant):

$$u_b(s) = i_b(s)R_b + \frac{R_p i_b(s)}{\tau_p s + 1} + U_{oc}(s), \tag{1}$$

wherein all parameters of the above model may depend on the battery temperature ϑ_b, battery current i_b and its state-of-charge ξ, which is defined in the following manner:

$$\xi = \frac{1}{Q_b(I_b)} \int i_b dt, \tag{2}$$

where the battery charge capacity Q_b may also depend on the average battery current load I_b (Pavković et al. 2017).

The parameters of the above battery dynamic model have been obtained by means of experimental identification carried out by Pavković et al. (2015). Figure 2a shows the experimentally-obtained OCV versus SoC profile $U_{oc}(\xi)$ of the considered 100 Ah $LiFePO_4$ battery cell (GWL/Power Group 2020), with individual $U_{oc}(\xi)$ voltage points obtained by successively discharging the battery from

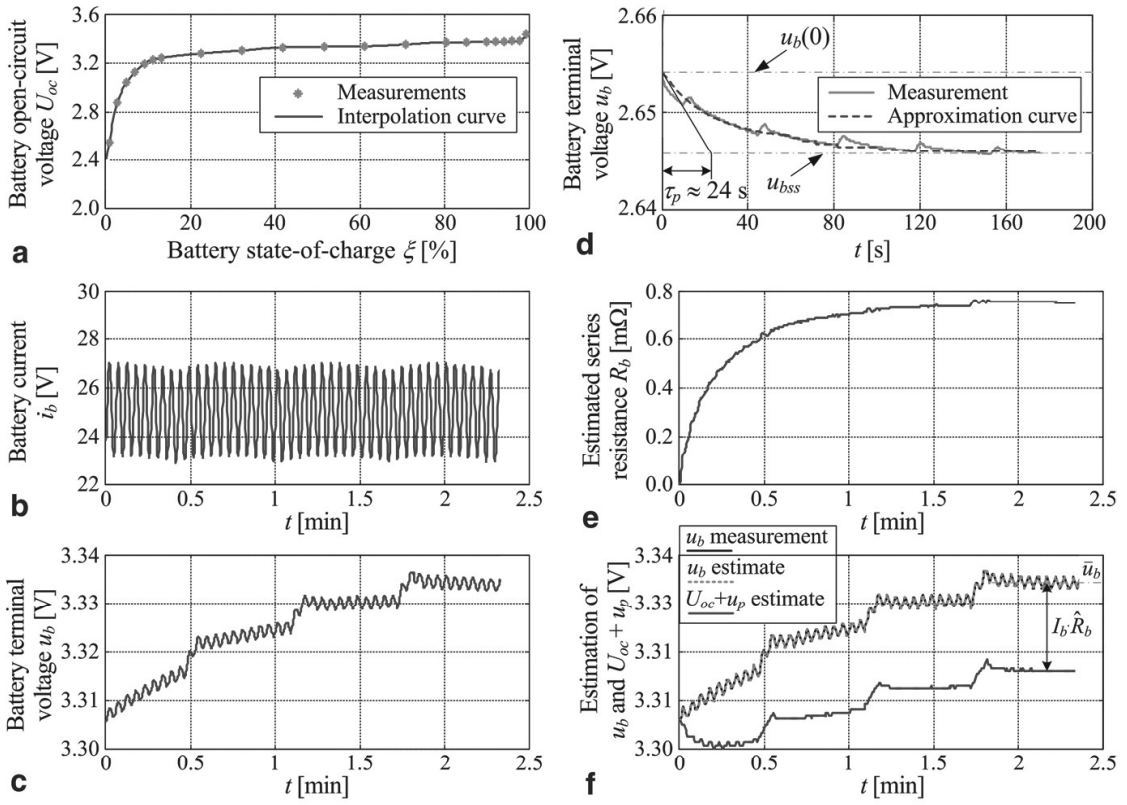

Fig. 2 Experimentally-recorded open-circuit voltage versus state-of-charge map of 100 Ah LiFePO4 battery (**a**), experimental traces of battery current (**b**) and terminal voltage (**c**) used for experimental identification, battery terminal voltage settling transient after battery current drops to zero (**d**), and results of series resistance estimation (**e**) and polarization voltage estimation (**f**)

the fully charged-state by a certain amount of charge at rather low discharging current ($I_b = 10$ A), interspersed by a at least two-hour resting periods. The corresponding battery terminal voltage u_b and state-of-charge ξ (calculated according to Eq. (2)) at the end of each resting period are recorded as a single $U_{oc}(\xi)$ point. The procedure is performed until the battery terminal voltage at rest drops below 2 V which is the minimum safe discharged voltage according to the manufacturer (GWL/Power Group 2020). It should also be noted that $U_{oc}(\xi)$ points are more densely recorded in the regions where larger battery terminal voltage u_b (and also U_{oc}) variations are expected, that is near the fully-charged and fully-discharged state in order to accurately capture the $U_{oc}(\xi)$ trend. Thus obtained $U_{oc}(\xi)$ points are then interpolated in order to produce a high-resolution $U_{oc}(\xi)$ map (look-up table). The polarization equivalent time constant, identified using the zero-current battery terminal voltage transient (Fig. 2d) has not shown significant variation with the operating point, so its average value $\tau_p = 24$ s is used in the analysis and subsequent design of the battery SoC estimator (Pavković et al. 2017).

Identification of battery equivalent circuit model resistance parameters, i.e. series resistance R_b and polarization resistance R_p in (Pavković et al. 2015) has been based on the quasi steady-state behavior of the battery equivalent circuit model subject to small-magnitude perturbations of the battery current i_b during constant-current charging and discharging, as illustrated by experimental traces

in Fig. 2b for the case of battery charging with average current of 25 A, with superimposed ± 2 A current variations. This charging current profile results in battery terminal voltage exhibiting variations proportional to variations of battery current, along with a slow upwards trend due to the slow dynamics of the polarization voltage and OCV (Fig. 2c). These slow dynamics can be effectively removed from the measurement signals by means of differentiation, thus resulting in the following simple model of battery terminal voltage variations Δu_b due to battery current variations Δi_b (k is the sampling step)

$$\Delta u_b(k) = \Delta i_b(k) R_b(k), \tag{3}$$

with battery voltage and current variations calculated as:

$$\Delta u_b(k) = u_b(k) - u_b(k-1), \tag{4}$$

$$\Delta i_b(k) = i_b(k) - i_b(k-1). \tag{5}$$

The above model (3) can be rewritten in the form of a regression model suitable for parameter estimator design, which has been realized as a first-order Kalman filter and used for the estimation of series resistance by Pavković et al. (2013):

$$P(k) = P(k-1) - K(k-1)\Delta i_b(k-1)P(k-1) + Q_p(k-1), \tag{6}$$

$$K(k) = \frac{P(k)\Delta i_b(k)}{P(k)\Delta i_b^2(k) + r_m(k)}, \tag{7}$$

$$\hat{R}_b(k) = \hat{R}_b(k-1) + K(k)\left[\Delta u_b(k) - \Delta i_b(k)\hat{R}_b(k-1)\right], \tag{8}$$

where $Q_p(k–1)$ is the desired variance of estimated parameter perturbations, $r_m(k)$ is the variance of measurement noise, $P(k)$ is the variance of parameter estimation error, $K(k)$ is the estimator measurement correction (update) gain, and $\hat{R}_b$ is the estimated series resistance, whose steady-state value is associated with the actual battery SoC ξ. This procedure is then repeated over the considered range of battery SoC operating points in order to define the battery series resistance versus SoC map (look-up table) $R_b(\xi)$.

Finally, based on the estimated series resistance R_b, the polarization resistance R_p is estimated from the steady-state part of the estimator response (see Fig. 2e and f) based on the following relationship:

$$U_{oc}(\xi) + \overline{u}_p(\xi) = U_{oc}(\xi) + I_b\hat{R}_p(\xi) = \overline{u}_b - I_b\hat{R}_b(\xi), \tag{9}$$

which finally yields:

$$\hat{R}_p(\xi) = \frac{\overline{u}_b - U_{oc}(\xi)}{I_b} - \hat{R}_b(\xi), \tag{10}$$

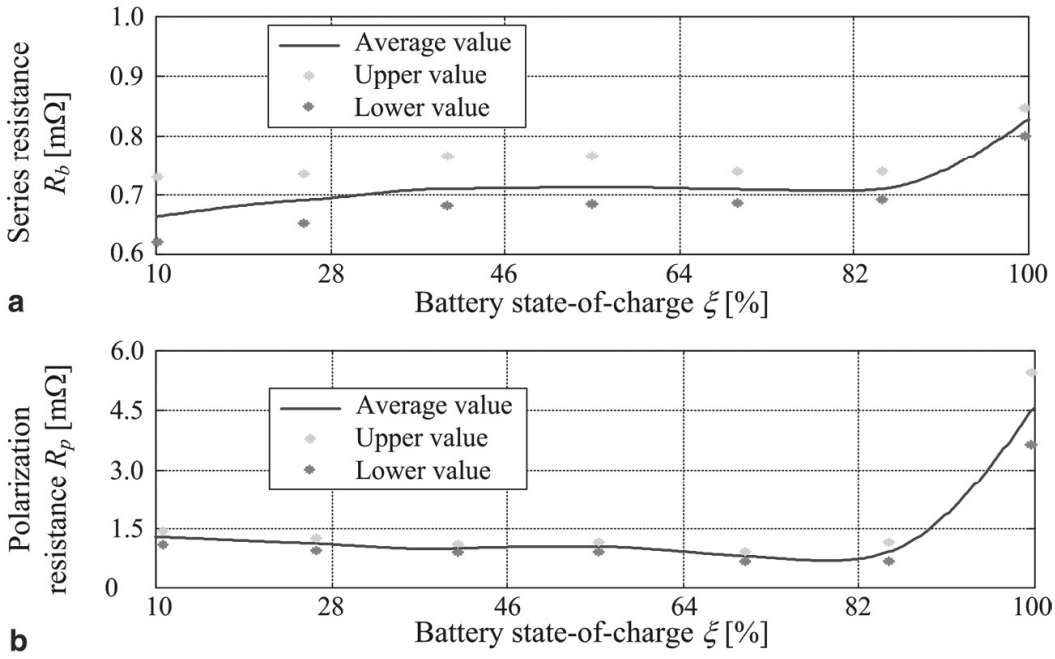

Fig. 3 Experimentally-recorded averaged maps of 100 Ah $LiFePO_4$ battery cell state-of-charge dependent series resistance (**a**), and polarization resistance (**b**)

where $\overline{u}_p(\xi)$ and $\hat{R}_p(\xi)$ are the steady-state polarization voltage and estimated polarization resistance for the particular SoC, and $\overline{u}_b$ and I_b are battery terminal voltage and current average values.

Figure 3 shows the dependences of averaged equivalent circuit model resistance parameters, with respect to SoC for the case of battery charging (Pavković et al. 2015). Averaged profiles of battery polarization and equivalent series resistance $R_p(\xi)$ and $R_b(\xi)$ with their respective upper and lower values (Pavković et al. 2015) are shown in Figs. 3a and b respectively. As expected, the SoC dependences of these parameters are more emphasized for boundary SoC values, especially for the fully-charged battery cell ($\xi \approx 1$). As shown by Pavković et al. (2016), series and polarization resistance parameters have shown only a mild dependence on average battery current, as indicated by the boundary (upper and lower) values in Fig. 3a and b.

2.2 Buck-type DC/DC converter

Right-hand-side in Fig. 1 shows the topology of buck converter comprising the active (switching) element (MOSFET Q) feeding the inductor (characterized by its inductance L_c and resistance R_c) and parallel-connected freewheeling diode D. The average value of voltage feeding the inductor can be calculated in the ideal case (negligible voltage drops on the MOSFET switch Q and the freewheeling diode D) based on the commanded pulse-width modulation (PWM) duty cycle d and DC supply voltage u_{dc} as follows (Williams 1992):

$$\overline{u}_c = du_{dc}, \tag{11}$$

so that the voltage balance equation over the inductor reads:

$$L_c \frac{di_c}{dt} + R_c i_c = \overline{u}_c - u_b. \tag{12}$$

In the above model, the PWM switching delay (dead-time) between the PWM duty cycle reference and the actual output voltage duty cycle value (due to finite PWM switching frequency f_{pwm}) may be approximated by the following first-order lag term (Isermann 1989):

$$G_{pc}(s) = \frac{1}{T_{pc}s + 1}, \tag{13}$$

where the lag time constant is equal to the reciprocal value of PWM switching frequency ($T_{pc} = 1/f_{pwm}$).

3 Control system design

This section presents the results of battery charging control system design, which is based on the cascade control system structure for controlling the battery current and limiting the battery terminal voltage, as well as controlling the battery SoC based on a dedicated EKF-based SoC estimator. The cascade control system design has been carried out based on the damping optimum criterion.

3.1 Damping optimum tuning procedure

The feedback controller tuning is based on the damping optimum criterion (Naslin 1968), which is a pole-placement-like method of designing linear continuous-time control systems with a full or reduced-order controller using the following formulation of the closed-loop system characteristic polynomial:

$$A_c(s) = D_2^{n-1} D_3^{n-2} \cdots D_n T_e^n s^n + \cdots + D_2 T_e^2 s^2 + T_e s + 1, \tag{14}$$

where T_e is the closed-loop system equivalent time constant, and D_2, D_3,…, D_n are the so-called characteristic ratios. In the optimal case $D_i = 0.5$ ($i = 2 \ldots n$), the closed-loop system of any order n has a quasi-aperiodic step response characterized by an overshoot of approximately 6% (resembling a second-order system with damping ratio $\zeta = 0.71$) and the approximate rise time $(1.8–2.1)\cdot T_e$. For larger T_e value choices, the dominant closed-loop modes are characterized by slower response, which generally improves the control system robustness and decreases the noise sensitivity. The response damping can be adjusted through varying the characteristic ratios D_2, D_3, …, D_n. In particular, the damping of dominant closed-loop modes is determined by the most dominant characteristic ratio D_2, with their damping being

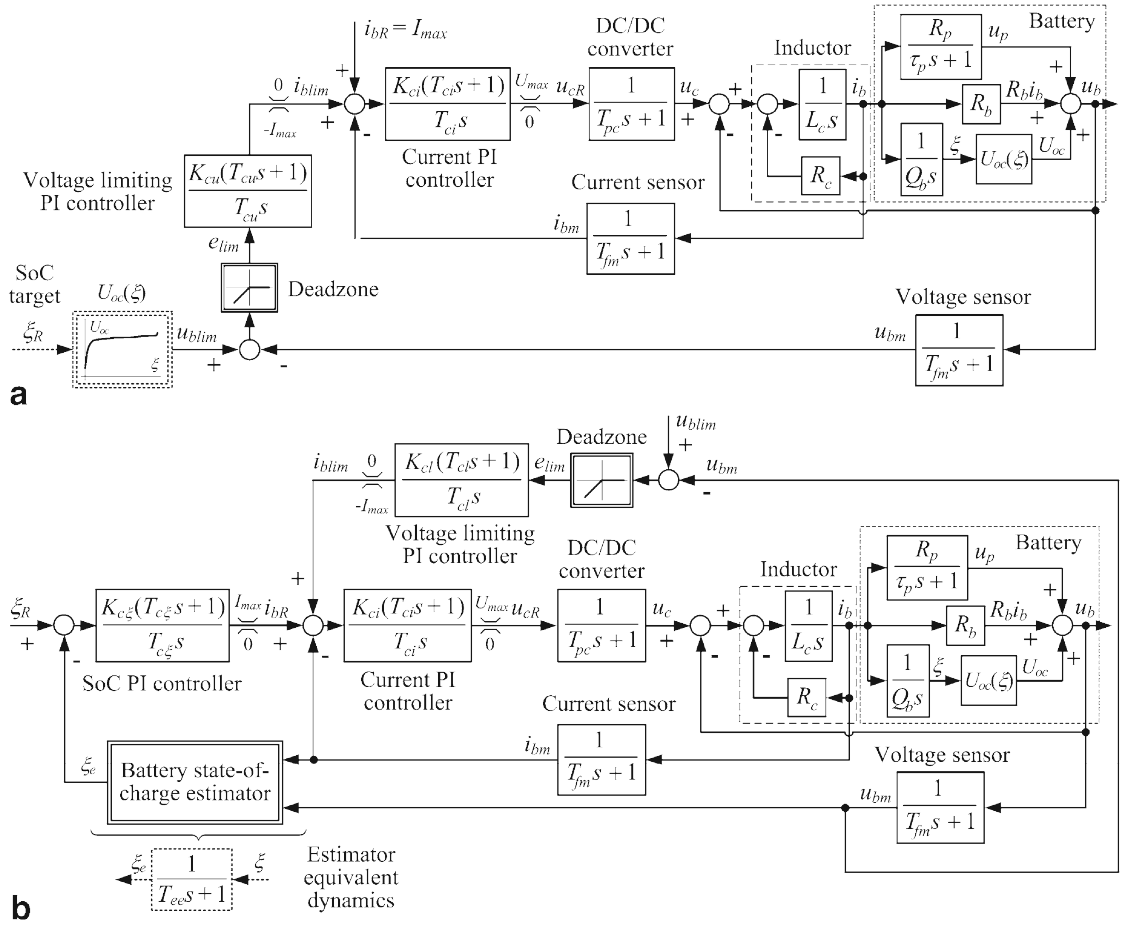

Fig. 4 Cascade control system arrangements used for battery charging based on inner current control loop: with battery terminal voltage limiting superimposed controller (**a**) and with dual state-of-charge/battery terminal voltage limiting superimposed controllers (**b**)

increased through reducing of the characteristic ratio D_2 below the optimal value 0.5, and vice versa (Naslin 1968).

3.2 Battery charging control systems

Figure 4 shows the block diagrams of the two considered battery charging control systems arranged in the so-called cascade control system, wherein the superimposed controller commanding the inner control loop effectively constrain the inner control loop output by means of limiting the reference commanded by the superimposed controller (or controllers). Additional benefits of cascade control approach include the control system modularity and straightforward switching between constant-current and constant-voltage operating modes (Pavković et al. 2014), as well as the straightforward control system design wherein the inner control loop is designed first, followed by the outer control loop design (Schröder 2007).

Figure 4a shows the control system structure for constant-current/constant voltage (CCCV) battery charging based on the inner current control loop with battery terminal voltage limiting outer feedback loop (denoted herein as the CCCV-VL

control), wherein both feedback loops feature proportional-integral (PI) feedback controllers. In this control system arrangement, which may be considered as a state-of-the-art benchmark case according to Hussein and Batarseh (2011) and Chen and Rincón-Mora (2006), the inner current control loop receives the current reference i_{bR} as a sum of the maximum charging current I_{max} used during the constant-current stage of the charging process and the negative current command i_{blim} from the superimposed voltage limiting controller, which is activated when the battery terminal voltage measurement u_{bm} exceeds the battery voltage limit value u_{blim} (dead-zone block in Fig. 4a). This battery terminal voltage limit value also effectively determines the battery SoC at the end of the charging process through the a-priori known OCV versus SoC dependence $U_{oc}(\xi)$, as indicated in Fig. 2a. More precisely, in this control system arrangement, the battery terminal voltage asymptotically approaches the desired state-of-charge related open-circuit voltage $U_{oc}(\xi)$ as the battery charging current i_b approaches zero (see e.g. discussion by Pavković et al. 2014).

Figure 4b shows the control system structure with the inner current control loop being commanded by two superimposed controllers denoted herein as the CCCV-SoC control approach. The principal state-of-charge controller commands an appropriate current reference (limited to the maximum allowed current value I_{max} during the constant current charging phase) based on the estimated battery state of charge value provided by a suitable estimator. The auxiliary battery terminal voltage limiting controller performs the same function as in the case of CCCV-VL control approach, with the comparative advantage of battery terminal voltage limit u_{blim} being preset independently of battery state-of-charge target (which has not been the case with the CCCV-VL control approach). From the standpoint of control system design, it is assumed that the dynamics of the battery state-of-charge estimate ξ_e (obtained by utilizing battery terminal voltage and charging current measurements u_{bm} and i_{bm} for SoC estimation) with respect to the actual battery SoC ξ can be approximated by a first-order lag term with the equivalent time constant T_{ee} (see Fig. 4b, and discussion in the next section):

$$G_e(s) = \frac{\xi_e(s)}{\xi(s)} \approx \frac{1}{T_{ee}s + 1}. \tag{15}$$

The above control system structures indicate that the CCCV-SoC strategy is a derivative of the traditional (and much simpler) CCCV-VL strategy, wherein the modularity of the proposed approaches means that CCCV-VL strategy can be augmented by a SoC control loop in a straightforward way, thus enabling the use of the more flexible CCCV-SoC charging strategy. Moreover, both the CCCV-VL strategy and the CCCV-SoC strategy ought to be applicable to any battery chemistry, provided that the charging current and terminal voltage ratings are available (e.g. from the manufacturer's data) for the CCCV-VL part of the control strategy, and that the battery equivalent circuit model and charge capacity are available for the design of the SoC estimator, which is needed for the implementation of the SoC control loop within the CCCV-SoC control strategy. Finally, both control strategies utilize rather straightforward PI controllers, whose design is also based on straightforward

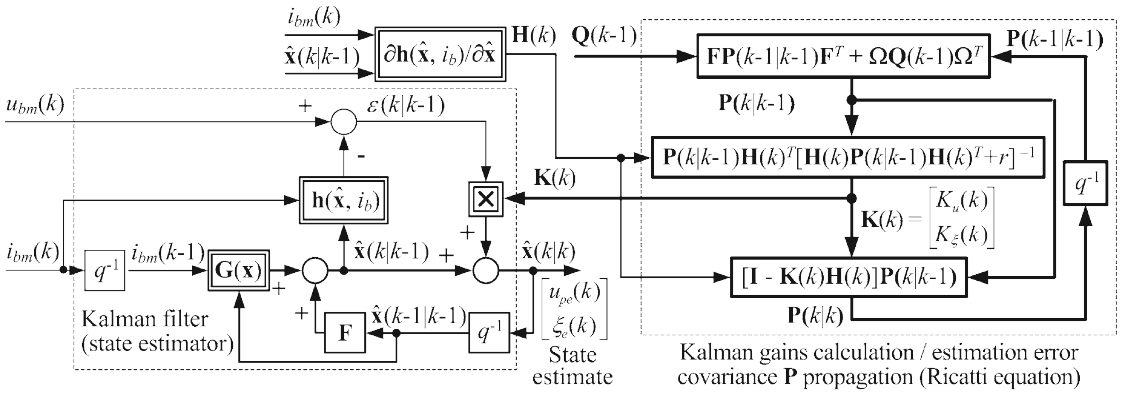

Fig. 5 Principal block diagram representation of extended Kalman filter for battery state-of-charge estimation

analytical tuning rules, which makes both control strategies well suited for practical applications.

3.3 State-of-charge estimator

Battery SoC estimation is based on the nonlinear battery model with a-priori known model parameters shown in Figs. 2 and 3, which are integrated within an EKF-based state estimator (Grewal and Anderson, 2001), whose principal block diagram is shown in Fig. 5. It consists of two parts, i.e. the state-variable estimator part (left-hand-side of Fig. 5) based on available battery terminal voltage and current measurements and the battery dynamic model given in its state-space form, and the optimal (Kalman) gain calculation based on so-called Ricatti equation (Grewal and Anderson 2001), wherein linearized battery process model is used to estimate the error covariance matrix $\mathbf{P}$, based on the assumed variances of state perturbations $\boldsymbol{\nu}$ (characterized by the perturbation covariance matrix $\mathbf{Q}$) and variance r of the noise e in the battery model output (i.e. battery terminal voltage measurement u_{bm}).

For the purpose of battery EKF-based state-of-charge estimator design, battery model is discretized in time and rewritten in the following state-space form (Pavković et al. 2017):

$$\underbrace{\begin{bmatrix} u_p(k) \\ \xi(k) \end{bmatrix}}_{x(k)} = \underbrace{\begin{bmatrix} a & 0 \\ 0 & 1 \end{bmatrix}}_{F} \underbrace{\begin{bmatrix} u_p(k-1) \\ \xi(k-1) \end{bmatrix}}_{x(k-1)} + \underbrace{\begin{bmatrix} (1-a)R_p(\xi(k-1)) \\ \frac{T}{Q_b} \end{bmatrix}}_{G(x(k-1))} i_{bm}(k-1) + \underbrace{\begin{bmatrix} T & 0 \\ 0 & T \end{bmatrix}}_{\Omega} \underbrace{\begin{bmatrix} \nu_u(k-1) \\ \nu_\xi(k-1) \end{bmatrix}}_{\nu(k-1)}, \tag{16}$$

$$u_{bm}(k) = \mathbf{h}(\mathbf{x}(k), i_b(k), e(k)) = u_p(k) + R_b(\xi(k))i_{bm}(k) + U_{oc}(\xi(k)) + e(k), \tag{17}$$

where the parameter a is related to the a-priori known polarization time constant τ_p and estimator sampling time T as follows:

$$a = e^{-T/\tau_p}. \tag{18}$$

As shown in Fig. 5, the EKF-based SoC estimator utilizes the deterministic part of the process model given by (16) and (17) to calculate the initial (so-called a-priori) state estimate $\hat{\mathbf{x}}(k|k-1)$. This initial state estimate is then updated based on the estimator output a-priori prediction error $\varepsilon(k|k\text{-}1)$ between the battery terminal voltage measurement and the deterministic part of the battery model output in expression (17) as follows:

$$\varepsilon(k|k-1) = u_{bm}(k) - \mathbf{h}\left(\hat{\mathbf{x}}(k|k-1), i_{bm}(k), 0\right), \tag{19}$$

with the state update given as the product of EKF gain vector $\mathbf{K}(k) = [K_u(k)\ K_\xi(k)]^T$ and the a-priori prediction error $\varepsilon(k|k-1)$ (see Fig. 5).

The tuning parameters of the EKF-based SoC estimator relate to the expected variances of state variable stochastic perturbations modeled by a stochastic perturbation vector $\boldsymbol{\nu}$ in (16) and characterized by the corresponding covariance matrix $\mathbf{Q}$, and measurement noise e variance r. Since the latter can be obtained from the battery terminal voltage measurements, the elements of the diagonal state perturbation covariance matrix $\mathbf{Q}$ effectively determine the EKF-based estimator tracking ability and noise suppression. For the purpose of calculation of the optimal state update gain $\mathbf{K}(k)$, the battery model output equation needs to be linearized in the vicinity of the state vector operating point, thus yielding the following definition of the $\mathbf{H}(k)$ matrix (row vector) used in Ricatti equation in Fig. 5 (Pavković et al. 2017):

$$\mathbf{H}(k) = \left[\ 1\ \ \frac{\partial U_{oc}(\xi(k))}{\partial \xi(k)} + \frac{\partial R_b(\xi(k))}{\partial \xi(k)}\, i_{bm}(k)\right]. \tag{20}$$

3.4 Controller tuning

Current controller design is based on the assumption of very slow OCV and polarization dynamics (Pavković et al. 2014), which may be treated as a slow (steady-state) disturbance for the current control system. Moreover, the parasitic (fast dynamics) within the current control loop, which are due to PWM switching lag T_{pc} of the DC/DC converter and the fast current senor dynamics (time constant T_{fm}), can be effectively approximated by a single lag term with the equivalent time constant $T_{\Sigma i} = T_{pc} + T_{fm}$ (and which may also include the effects of time-discretization in the case when digital controller is used):

$$G_{par,i}(s) = \frac{1}{T_{\Sigma i}s + 1}. \tag{21}$$

Based on these approximations, the application of damping optimum criterion to the current control loop transfer function characteristic polynomial yields the following expression for the current controller parameters (i.e. closed-loop equivalent time constant T_{ei}, and PI controller proportional gain K_{ci} and integral time constant T_{ci}):

$$T_{ei} \geq T_{ei,min} = \frac{1}{D_{2i}D_{3i}} \frac{T_{\Sigma i}}{1 + T_{\Sigma i}(R_c + R_b)/L_c}, \tag{22}$$

$$T_{ci} = T_{ei}\left(1 - \frac{D_{2i}T_{ei}}{T_{\Sigma i} + L_c/(R_c + R_b)}\right), \tag{23}$$

$$K_{ci} = \left(R_c + R_b\right)\left(\frac{T_{\Sigma i} + L_c/\left(R_c + R_b\right)}{D_{2i}T_{ei}} - 1\right). \tag{24}$$

Similarly, for the case of battery terminal voltage limiting controller, the OCV and polarization dynamics are assumed to be rather slow, so that battery terminal voltage dynamic variations are primarily affected by the series resistance voltage drop (Pavković et al. 2014). As in the case of current controller design, the fast dynamics of the inner current control loop and the voltage sensor are approximated by a first-order lag term with equivalent time constant $T_{\Sigma u} = T_{ei} + T_{fm}$ comprising the equivalent current control loop lag T_{ei} and the voltage sensor lag T_{fm} (and time-discretization related delay in the case of digital controller):

$$G_{par,u}(s) = \frac{1}{T_{\Sigma u}s + 1}. \tag{25}$$

Based on the above approximation, the damping optimum criterion yields the following tuning expressions for the battery terminal voltage limiting PI controller parameters (i.e. controller proportional gain K_{cl} and integral time constant T_{cl}):

$$T_{cl} = T_{el}\left(1 - \frac{D_{2u}T_{el}}{T_{\Sigma u}}\right), \tag{26}$$

$$K_{cl} = \frac{1}{R_b}\left(\frac{T_{\Sigma u}}{D_{2u}T_{el}} - 1\right). \tag{27}$$

where the closed-loop equivalent time constant T_{el} is subject to the following feasibility constraint:

$$T_{el} < \frac{T_{\Sigma u}}{D_{2u}}. \tag{28}$$

As previously stated regarding the battery SoC estimator, it is assumed that the estimator SoC tracking ability is characterized by a time lag T_{ee}, which can be added to the overall lag of the inner current control loop according to Eq. (22). Thus, after applying the damping optimum criterion to the SoC control loop (and assuming that the battery terminal voltage controller is inactive), the following results are obtained for the case of SoC controller tuning:

Table 1 Key parameters of the simulation model

Parameter	Value
Inductor inductance L_c	0.7 mH
Inductor resistance R_c	50 mΩ
DC/DC converter lag $T_{pc} = 1/f_{pwm}$	1 ms
DC bus voltage for DC/DC converter u_{dc}	36 V
Current/voltage sensor time constant T_{fm}	5 ms
$LiFePO_4$ battery cell charge capacity Q_b	100 Ah
Battery charging current upper limit I_{max}	70 A
Battery charging turn-off current I_{min}	5 A
Battery terminal voltage limit u_{bmax}	3.5 V
Initial battery state-of-charge ξ_0	20%
Battery state-of-charge target value ξ_R	100%

Table 2 Parameters of the EKF-based state-of-charge estimator

Parameter	Value
Sampling time T	0.5 s
Measurement noise variance r	0.1 V^2
Q matrix first diagonal element **Q**(1,1)	0.001 V^2
Q matrix second diagonal element **Q**(2,2)	2.5 $(As)^2$
Q matrix cross-diagonal elements **Q**(1,2) = **Q**(2,1)	0.0

$$T_{c\xi} = T_{e\xi} \geq \frac{T_{ee} + T_{\Sigma u}}{D_{2\xi} D_{3\xi}}, \tag{29}$$

$$K_{c\xi} = \frac{Q_b}{D_{2\xi} T_{e\xi}}. \tag{30}$$

4 Simulation results

The two proposed battery charging control systems have been verified by means of simulations using the previously developed model of a $LiFePO_4$ battery cell, implemented within the Matlab/Simulink environment.

4.1 Simulation parameters

The key parameters of the simulation model are listed in Table 1, along with the key parameters of the proposed charging control strategies. In particular, the battery charging current upper limit I_{max} defines the maximum battery charging current

during the constant current charging phase, while the battery charging turn-off current I_{min} effectively determines the end-of-charging condition ($i_b < I_{min}$) in the constant-voltage charging regime. In practical applications it would be advantageous to set the battery terminal voltage limit below the technological voltage limit value (3.65 V according to GWL/Power Group 2020). In this simulation study, two battery voltage limits is used as the precaution against battery over-voltages: $u_{bmax} = 3.4$ V and $u_{bmax} = 3.5$ V, wherein the former value corresponds to charged battery ($\xi = 100\%$) according to the known OCV versus SoC characteristic in Fig. 2a (see the discussion in previous section) and can be used as a target value u_{blim} within the CCCV-VL control strategy. The latter value can either be used as the battery terminal voltage target u_{blim} within the CCCV-VL strategy or the explicit battery terminal voltage limit within the CCCV-SoC strategy.

Table 2 lists the parameters of the EKF-based SoC estimator, with sampling time T chosen based on the previous study presented by Pavković et al. (2017). The battery terminal voltage measurement noise variance $r = 0.1$ V^2 is chosen to facilitate rather favorable robustness to measurement noise, whereas the diagonal elements of the state perturbation covariance matrix $\mathbf{Q}$ are chosen to obtain favorable estimator tracking ability. On the other hand, the cross-diagonal elements of the $\mathbf{Q}$ matrix are set to zero, because it is assumed that state perturbations are independent (uncorrelated) Gaussian stochastic processes. For this set of estimator parameters, the

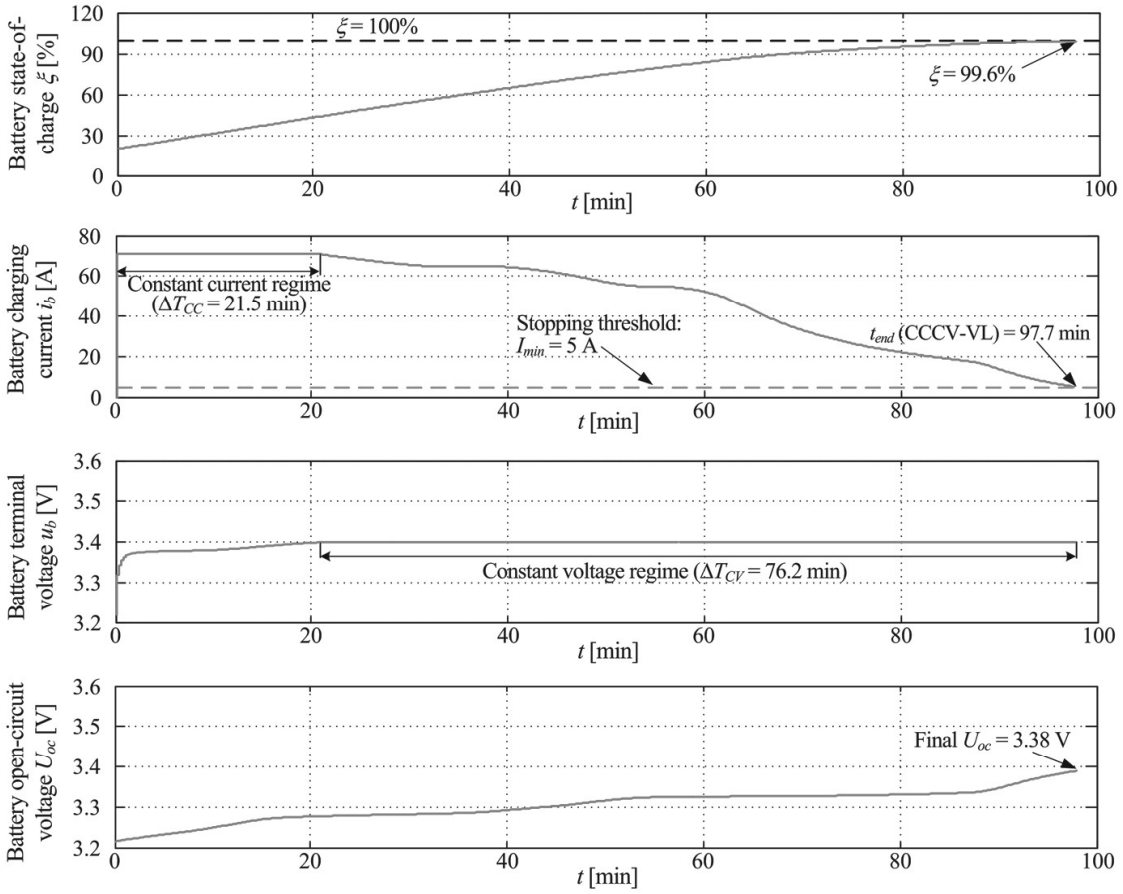

Fig. 6 Simulation results of CCCV-VL charging control strategy illustrating constant-current and constant-voltage battery charging regimes for battery terminal voltage limit set to 3.4 V

equivalent time constant of the estimator T_{ee} is estimated by means of simulations to $T_{ee} \approx 10$ s.

4.2 CCCV-VL charging strategy and SoC estimator tests

For the benchmark case of CCCV-VL control strategy, the battery terminal voltage limit u_{blim} has been set to 3.4 V, which corresponds to the fully-charged battery OCV $U_{oc}(\xi = 100\%)$, so the battery SoC ξ ought to be close to 100% at the end of the charging process. The SoC simulation traces in the top plot in Fig. 6 show that the battery SoC indeed reaches 99.6% at the end of the charging process, wherein end-of-charging is indicated by battery current dropping below the minimum current threshold $I_{min} = 5$ A (upper middle plot in Fig. 6). The battery charging current simulation traces also show that the constant-current regime (with maximum charging current $I_{max} = 70$ A) is maintained only during the first 21.5 min. The remainder of the charging process (lasting 97.7 min overall) is conducted in the constant voltage regime (see lower middle plot in Fig. 6), with the battery terminal voltage limited to $u_{blim} = 3.4$ V, as explained above. The OCV trace also confirms that the battery asymptotically approaches the fully-charged state, with the final reached value $U_{oc} = 3.38$ V due to the charging current termination condition being realized (i.e. battery current falling below the minimum value $I_{min} = 5$ A) before the battery is 100% charged ($U_{oc}(\xi = 100\%) = 3.4$ V).

Figure 7 shows the simulation results for the case of higher battery terminal voltage limit (voltage target) choice $u_{blim} = 3.5$ V. In this case, the constant-current charging regime is effectively prolonged so it lasts 62.4 min (middle plot

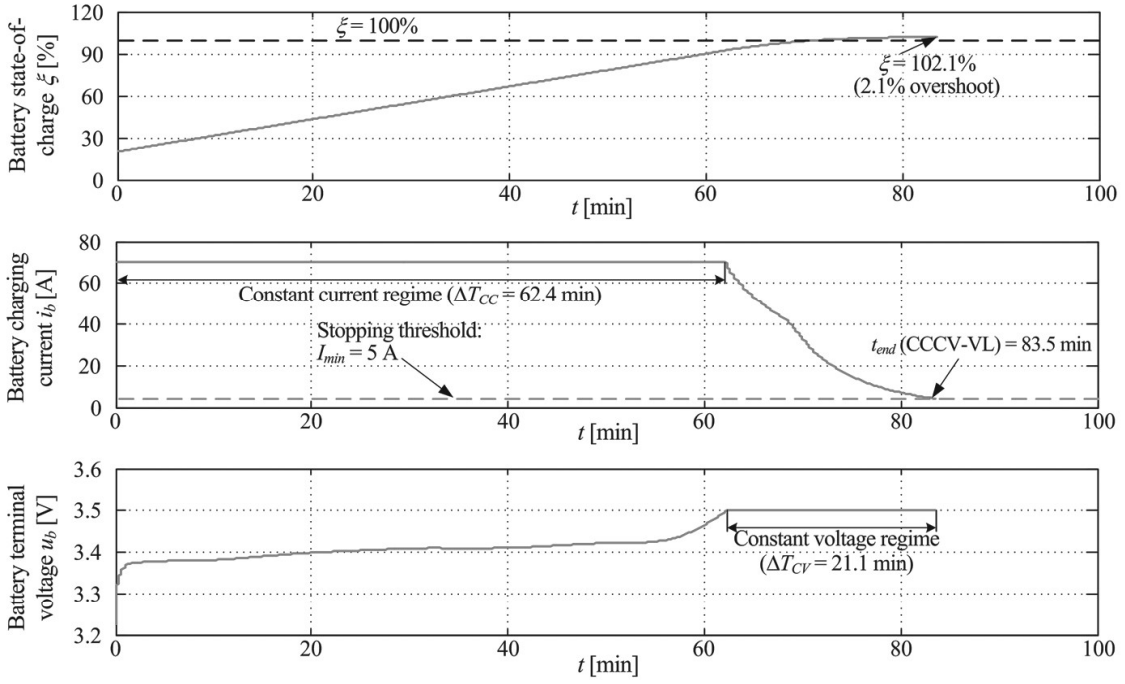

Fig. 7 Simulation results of CCCV-VL charging control strategy illustrating constant-current and constant-voltage battery charging regimes for battery terminal voltage limit set to 3.5 V

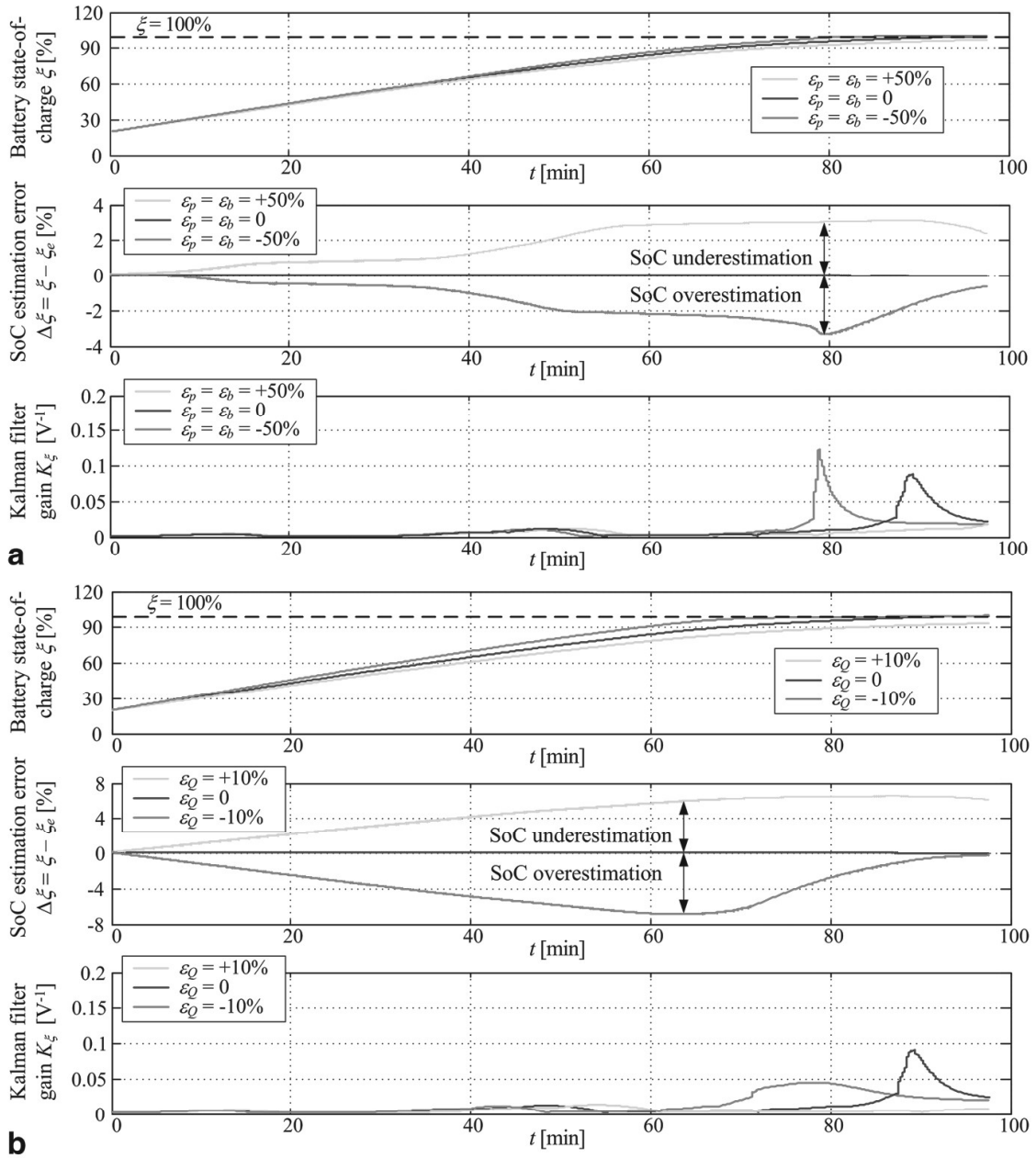

Fig. 8 Comparative results of battery SoC estimation under CCCV-VL control strategy and target battery terminal voltage $u_{blim} = 3.4$ V: effect of polarization and series resistance error (**a**), and charge capacity error (**b**)

in Fig. 7), while the constant-voltage regime duration is far shorter (21.1 min), as indicated by lower plot in Fig. 7. This results in battery recharging within 83.5 min, which represents a 14.5% speedup of the overall charging process. However, by choosing the battery terminal voltage target value larger than the full-charged OCV, the battery may become overcharged, which is indicated in the SOC trace (top plot in Fig. 7) showing a 2.1% overshoot compared to the ideal SoC ($\xi = 100\%$) after recharging. Naturally, this kind of charging regime would result in accelerated battery aging and should be avoided (Ehrlich 2002).

Figure 8 shows the results of the EKF-based estimation of the battery state of charge for the case of CCCV-VL charging control strategy with battery voltage target value $u_{blim} = 3.4$ V (simulation scenario in Fig. 6). The simulation study is carried out for the nominal case (no battery modeling errors in estimator design), and battery polarization and series resistance errors (Fig. 8a), and battery charge capacity errors (Fig. 8b), defined as follows:

$$R_{b,est} = R_b\left(1 + \varepsilon_b\right), \tag{31}$$

$$R_{p,est} = R_b\left(1 + \varepsilon_p\right), \tag{32}$$

$$Q_{b,est} = Q_b\left(1 + \varepsilon_Q\right). \tag{33}$$

where R_b, R_p and Q_b are nominal battery model parameters, $R_{b,est}$, $R_{p,est}$ and $Q_{b,est}$ are parameters used within the estimator and ε_b, ε_p and ε_Q are series and polarization resistance and charge capacity modeling errors, amounting to $\pm 50\%$ in the case of resistance errors and $\pm 10\%$ in the case of charge capacity error.

The aforementioned battery modeling errors result in drift-like behavior of SoC estimation error, visible as discrepancy between the nominal case (blue traces in top plots in Fig. 8a and b). SoC tracking error plots in Figs. 8a and b indicate the SoC overestimation is characteristic for the case of underestimated battery internal resistances and charge capacity (ε_p, ε_b, $\varepsilon_Q < 0$), while SoC underestimation occurs in the case of overestimated battery model parameters within the estimator (ε_p, ε_b, $\varepsilon_Q > 0$), when compared to the nominal case characterized by negligible SoC tracking error. The aforementioned drift-like behavior of SoC estimation error appears to be more pronounced in the middle of the charging process, characterized by rather large charging currents, whereas the SoC estimation error tends to diminish near the end of the charging process (i.e. at relatively small charging currents). Namely, in that case the EKF-based estimator appears to rely more on the battery terminal voltage measurement to reconstruct the battery SoC from the known (and reliable) $U_{oc}(\xi)$ characteristic, i.e. $i_{bm} \to 0$, $u_{bm} \to U_{oc}(\xi)$ according to Eq. (1). This is further indicated by Kalman filter gain K_ξ traces in bottom plots in Fig. 8a and b, which tend to increase at the end of the charging process. Thus, the SoC estimation error may even diminish towards zero at the end of the charging process, especially in the case of battery model parameters underestimation (ε_p, ε_b, $\varepsilon_Q < 0$) within the EKF-based estimator.

4.3 CCCV-SoC strategy results

Figure 9 shows the comparative simulation results of the presented CCCV-VL and CCCV-SoC control strategies. Again, for the benchmark case of CCCV-VL control strategy, the battery terminal voltage limit u_{blim} has been set to 3.4 V corresponding to the fully-charged battery OCV $U_{oc}(\xi = 100\%)$. When the CCCV-SoC control strategy is employed, along with the more flexible choice of the battery terminal voltage

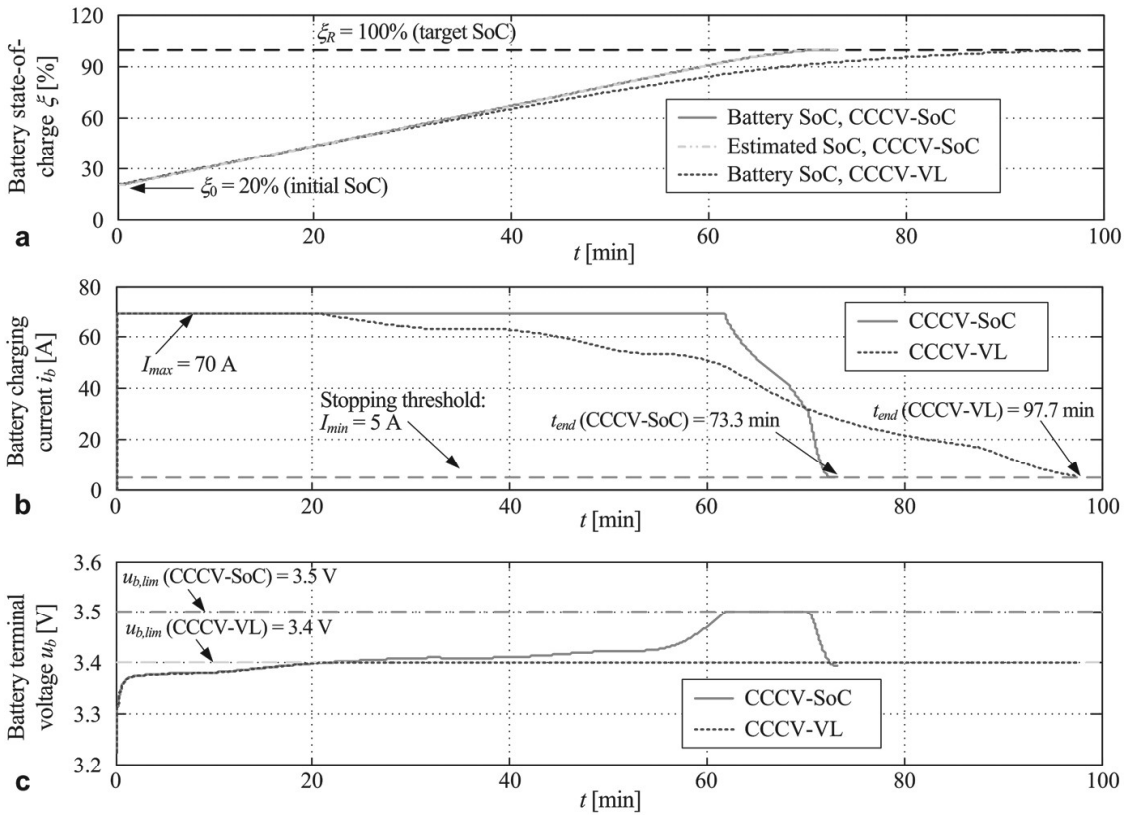

Fig. 9 Comparative results of CCCV-VL and CCCV-SOC control strategies: battery SoC target, measurement and estimate (**a**), battery charging current traces (**b**) and battery terminal voltage responses (**c**)

limit $u_{blim} = u_{bmax} = 3.5$ V (bottom plot in Fig. 9), the charging process is effectively speeded-up when compare to the CCCV-VL benchmark case due to the constant-current regime being maintained for over 60 min (red trace in the middle plot in Fig. 9). This, in turn results in 100% of battery SoC being reached within 73.3 min (top plot in Fig. 9), which corresponds to 25% speed-up of the overall charging process when CCCV-SoC approach is used. Moreover, in the CCCV-SoC approach, the duration of the constant-voltage regime is much shorter in turn, i.e. the battery terminal voltage limit value is maintained for a shorter period of time. These results clearly indicate that by independently controlling the battery SoC using a precise battery SoC estimator (cf. red and green dotted traces in the top plot in Fig. 9), and having an additional degree-of-flexibility with respect to battery terminal voltage limitation, a more effective battery charging process can be carried out by using the CCCV-SoC approach compared to the conventional approach (CCCV-VL) using constant current charging with fixed-valued battery terminal voltage limiting.

Finally, the battery charging system based on the CCCV-SoC control strategy has been tested for the case of battery modeling errors. In particular, the simulation scenario related to battery internal resistance modeling errors (ε_p, ε_b) is chosen to illustrate the level of robustness, wherein the case of underestimated battery resistance parameters (ε_p, $\varepsilon_b < 0$) would relate to aged battery or battery operation at low temperatures, whereas overestimated resistance parameters (ε_p, $\varepsilon_b > 0$) would indicate battery operating at higher temperatures (Ehrlich 2002).

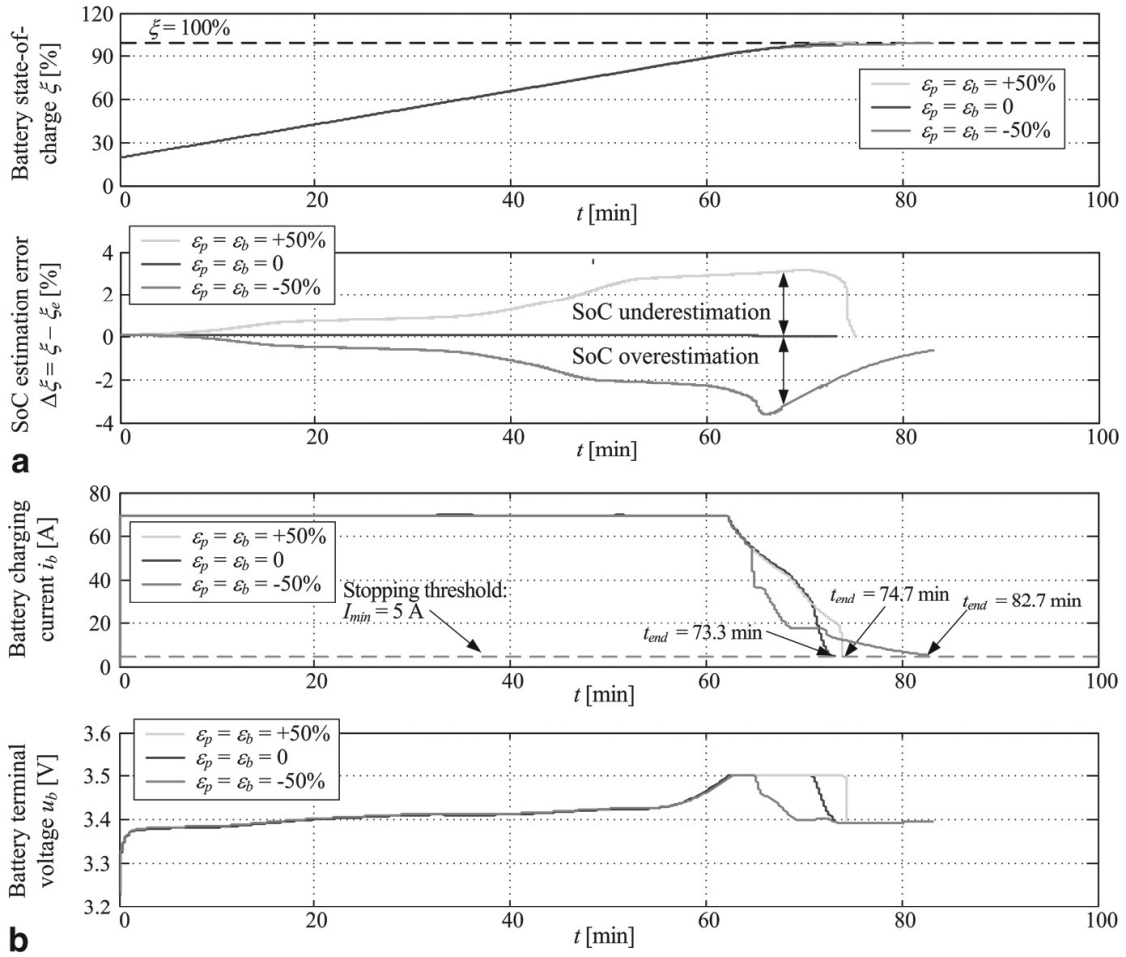

Fig. 10 Comparative results of battery charging using CCCV-SoC control strategy with battery terminal voltage limit $u_{blim} = 3.5$ V subject to polarization and series resistance error: SoC traces and SoC estimation errors (**a**) and battery current and voltage traces (**b**)

Simulation results for the case of $\pm 50\%$ error in series and polarization resistance parameters are shown in Fig. 10. When compared to the nominal case (no resistance modeling errors within the estimator), modeling errors generally result in the somewhat longer charging duration. In the case of resistance parameter overestimation (ε_p, $\varepsilon_b > 0$) and resulting SoC underestimation (bottom plot in Fig. 10a), the SoC controller maintains the constant-voltage charging interval somewhat longer (bottom plot in Fig. 10b). However, the charging process is abruptly ended when the limited battery terminal voltage (limited to 3.5 V) can no longer support the charging current, thus resulting in only a 1.2 min charging duration increase compared to the nominal case (top plot in Fig. 10b). On the other hand, when the resistance parameters are underestimated (ε_p, $\varepsilon_b < 0$), the effective charging duration is increased because of the SoC overestimation within the EKF (Fig. 10a), which results in the SoC controller commanding a lower current reference in order to prevent the perceived battery overcharging and lowering the battery terminal voltage in the process (Fig. 10b). In both of the considered cases there is no perceptible overshoot in the closed-loop controlled SoC

response. This is likely due to the aforementioned EKF estimator tendency to rely more on the battery voltage measurement for SoC reconstruction at the end of the charging process.

5 Summary and discussion of results

The presented simulation results of the presented cascade control system designs and related battery charging strategies without and with explicit SoC control based on EKF-based SoC estimator have indicated the following:

- Both the conventional CCCV-VL battery control strategy using an inner current controller commanded by the superimposed-level battery terminal voltage limiting controller and the advanced SoC controller-based (CCCV-SoC) charging strategy are able to accurately recharge the battery, with the CCCV-SoC strategy being able to achieve 25% speedup compared to the CCCV-VL strategy when recharging from 20% SoC to the fully-charged battery state (100% SoC).
- Speeding up the CCCV-VL strategy by increasing the battery terminal voltage target value may result in battery overcharging, which should be avoided in order to prolong the battery useful cycle life.
- SoC estimator may be sensitive to battery equivalent circuit model parameter errors, which result in drift-like SoC estimation error. This estimation error, though, appears to decrease as the charging process nears its completion due to the EKF-based estimator relying more on the battery terminal voltage measurement as the charging current decreases towards zero.
- The CCCV-SoC control strategy appears to be moderately robust to battery modeling errors in terms of charging duration and accuracy of the final SoC for the considered $\pm 50\%$ variation of the battery model resistance parameters. However, this may not be the case in the case of larger battery model discrepancies.

Based on these insights, the CCCV-SoC control system is capable of achieving a perceptible speedup of the battery charging process (up to 25% faster charging)

Table 3 Comparison of charging process speedup for different charging strategies

Charging method (reference)	Speedup versus CCCV (%)
Fuzzy logic controller with safe voltage limiting (Hsieh et al 2001)	13.2
MCC charging with offline optimization (Vo et al. 2015)	19.1 to 29.7
Model predictive control with moving horizon estimation (Zou et al. 2018)	17.5
Genetic algorithm for offline optimization plus MCC charging (Jian et al. 2021)	39.7
LMS online estimator combined with MCC charging (Rai et al. 2020)	39.3
EKF-based charging control/CCCV-SoC (proposed method)	25

when compared to the conventional CCCV-VL control strategy, while also being reasonably robust to moderate error of battery process model parameters within the EKF-based SoC estimator. Further improvements of the CCCV-SoC control strategy robustness may include more detailed maps of battery model parameters within the EKF-based estimator, or, alternatively, online parameter adaptation of the SoC estimator.

The charging process speedup result obtained herein is also compared with the results of other advanced charging control techniques from the available literature. In particular, charging speedup results are summarized in Table 3, which lists relative reductions of charging time with respect to the traditional CCCV technique. These results show that the CCCV-SoC control strategy proposed herein largely surpasses the charging speed performance compared to the fuzzy logic control-based approach (Hsieh et al. 2001), multi-level constant current charging (MCC) with offline optimization of the charging trajectory (Vo et al. 2015) and model predictive control with moving horizon estimation of the battery SoC (Zou et al. 2018). The proposed method is apparently less effective when compared to MCC charging based on offline optimization utilizing genetic algorithm for charging trajectory generation (Jian et al. 2021), and MCC charging based on LMS estimator of the battery OCV (Rai et al. 2020). The latter methods, however, either require extensive searching for the optimal parameters of the charging current trajectory (Jian et al. 2021), or an additional dynamic excitation signal to identify the battery OCV in real-time in order to use this information for SoC determination based on the a-priory known OCV versus SoC curve (Rai et al. 2020). The latter methods, although highly effective in terms of battery charging process speedup, may be relatively complex to implement, especially when considering the offline optimization requirement as shown by Jian et al. (2021). On the other hand, the CCCV-SoC methodology proposed in this work is designed to be modular, i.e. it is devised with the aim to augment the traditional (CCCV-VL) charging control strategy in a straightforward manner, while also having simple analytical tuning rules for each controller. Thus, the proposed CCCV-SoC control strategy ought to be fairly simple to implement, which is desirable from the standpoint of practical application.

6 Conclusion

The paper has presented two designs of constant-current/constant voltage battery charging control systems based on the cascade control system arrangement, and featuring a common inner current control loop based on a traditional PI controller. The superimposed control level, which commands the inner current control loop reference (target) has been realized in two distinct forms, depending on the availability of battery SoC information, that is (i) battery terminal voltage limitation control loop (conventional or CCCV-VL approach), and (ii) utilization of an outer battery SoC control loop based on EKF for SoC estimation, using the existing (auxiliary) battery terminal voltage controller for preventing battery over-voltages (herein referred to as CCCV-SoC control strategy). In this sense, the overall charging control system is highly modular, i.e. the CCCV-SoC strategy is simply an extension of the traditional

CCCV-VL charging strategy with an additional SoC control loop. The control system design has been based on the damping optimum criterion, and the effectiveness of the proposed battery charging control systems has been verified by means of simulations featuring a $LiFePO_4$ battery cell model.

Simulation results have shown that the CCCV-SoC control strategy has a distinct advantage over the more traditional CCCV-VL charging strategy due to the former having an additional degree of freedom through simultaneous control of battery SoC and independent battery terminal voltage limitation. In this sense, the CCCV-SoC strategy is able to maintain higher constant-valued battery terminal voltage limit without affecting the end result, i.e. the final battery SoC thus also enabling longer duration of the constant-current charging phase compared to the CCCV-VL control strategy. This ultimately results in notably faster battery re-charging from the initial deeply discharged state (SoC = 20%) to the fully charged state (SoC = 100%). In particular, the proposed CCCV-SoC control strategy has shown notable potential for speedup of the charging process, with charging duration reduced by 25% compared to the case of conventional CCCV-VL charging strategy.

In the case of notable discrepancies between the battery cell equivalent circuit parameters (i.e. its series and polarization resistance and charge capacity) and used within the battery the EKF-based SoC estimator and the battery itself, parameter value overestimation generally results in SoC underestimation and vice versa. Due to the inherent feature of the EKF-based SoC estimator which relies more on the battery terminal voltage measurement as the battery charging current drops towards zero (i.e. during the constant-voltage charging phase), the SoC estimator error decreases as the charging process nears its completion. Hence, for the case of moderate battery modeling errors, the final SoC may closely match the desired SoC value in the case when CCCV-SoC strategy is used. However, this may not be the case if the modeling errors are more pronounced, thus meriting further research.

Future work will be directed towards further battery modeling for advanced batteries such as those based on lithium-titanate chemistries and experimental verification of subsequently developed estimation and control strategy designs on the dedicated test setup which is currently under development. Analysis of battery parameter variations to SoC estimation accuracy within the charging control strategy is also going to be further investigated.

Acknowledgements It is gratefully acknowledged that this research has been supported by the European Regional Development Fund under Grants KK.01.1.1.01.0009 (DATACROSS) and KK.01.1.1.04.0010 (HiSkid), and by the European Commission through the Horizon 2020 project "Maximizing the impact of innovative energy approaches in the EU islands" (INSULAE). Authors also appreciate the efforts of the anonymous reviewers whose comments and suggestions have helped to improve the quality of the presented subject matter.

References

Abdel-Monem M, Trad K, Omar N, Hegazy O, Van den Bossche P, Van Mierlo J (2017) Influence analysis of static and dynamic fast-charging current profiles on ageing performance of commercial lithium-ion batteries. Energy 120:171–191

Afshar S, Morris K, Khajepour A (2019) State-of-charge estimation using an EKF-based adaptive observer. IEEE Trans Control Syst Technol 27(5):1907–1923

Ahmad S, Spiryagin M, Cole C, Wu Q, Wolfs P, Bosomworth C (2021) Analysis of positioning of wayside charging stations for hybrid locomotive consists in heavy train operations. Railw Eng Sci 23(3):285–298

Aziz M, Oda T, Ito M (2016) Battery-assisted charging system for simultaneous charging of electric vehicles. Energy 100:82–90

Buzzonii L, Pede G (2012) New prospects for public transport electrification. In: Proceedings of international conference on electrical systems for Aircraft, Railway and Ship propulsion (ESARS 2012), Bologna, Italy

Chen L-R, Liu C-S, Chen J-J (2009) Improving phase-locked battery charger speed by using resistance compensated technique. IEEE Trans Industr Electron 56(4):1205–1211

Chen Z, Xia B, Mi CC, Xiong R (2015) Loss-minimization-based charging strategy for lithium-ion battery. IEEE Trans Ind Appl 51(5):4121–4129

Chen M, Rincón-Mora GA (2006) Accurate, compact, and power-efficient li-ion battery charger circuit. IEEE Trans Circ Syst II Express Briefs 53(11):1180–1184

Chinese D, Pinamonti P, Mauro C (2021) A spatially explicit optimization model for the selection of sustainable transport technologies at regional bus companies. Optim Eng 22:1921–1954

Cipek M, Pavković D, Kljaić Z, Mlinarić TJ (2019) Assessment of battery-hybrid diesel-electric locomotive fuel savings and emission reduction potentials based on a realistic mountainous rail route. Energy 173:1154–1171

Cipek M, Pavković D, Krznar M, Kljaić Z, Mlinarić TJ (2021) Comparative analysis of conventional diesel-electric and hypothetical battery-electric heavy haul locomotive operation in terms of fuel savings and emissions reduction potentials. Energy 232:121097

Deur J, Škugor B, Cipek M (2015) Integration of electric vehicles into energy and transport systems. Autom J Control Meas Electron Comput Commun 56(4):395–410

Ehrlich GM (2002) Lithium-ion batteries. In: Linden D, Reddy TB (eds) Chapter 35 of handbook of batteries, 3rd edn. McGraw-Hill, New York

Fotouhi A, Auger DJ, Propp K, Longo S (2018) Accuracy versus simplicity in online battery model identification. IEEE Trans Syst Man Cybern Syst 48(2):195–206

Goodall G, Scioletti M, Zolan A, Suthar B, Newman A, Kohl P (2019) Optimal design and dispatch of a hybrid microgrid system capturing battery fade. Optim Eng 20:179–213

Grewal MS, Andrews AP (2001) Kalman filtering – theory and practice. Wiley, New York

GWL/Power Group (2020) SE100AHA cell specification, Technical data sheet http://www.ev-power.eu/CALB-40Ah-400Ah/SE100AHA-Lithium-Cell-LiFePO4-3-2V-100Ah.html. Accessed 20 Dec 2020

How DNT, Hannan MA, Hossain Lipu MS, Ker PJ (2019) State of charge estimation for lithium-ion batteries using model-based and data-driven methods: a review. IEEE Access 7:136116–136136

Hsieh G-C, Chen L-R, Huang K-S (2001) Fuzzy-controlled li-ion battery charge system with active state-of-charge controller. IEEE Trans Ind Electron 48(3):585–593

Huang C-S, Chow M-Y (2021) Robust state-of-charge estimation for lithium-ion batteries over full SoC range. IEEE J Emerg Sel Top Ind Electron 2(3):305–313

Hussein AAH, Batarseh I (2011) A review of charging algorithms for nickel and lithium battery chargers. IEEE Trans Veh Technol 60(3):830–838

Isermann R (1989) Digital control systems, vol 1. Springer, Berlin

James M, Grummett J, Rowan M, Newman J (2006) Application of pulse charging techniques to submarine lead-acid batteries. J Power Sources 162(2):878–883

Jiang J, Liu Q, Zhang C, Zhang W (2014) Evaluation of acceptable charging current of power li-ion batteries based on polarization characteristics. IEEE Trans Industr Electron 61(12):6844–6851

Jiang L, Huang Y, Li Y, Yu J, Qiao X, Huang C, Cao Y (2021) Optimization of variable-current charging strategy based on SOC segmentation for li-ion battery. IEEE Trans Intell Transp Syst 22(1):622–629

Lai X, Zheng Y, Sun T (2018) A comparative study of different equivalent circuit models for estimating state-of-charge of lithium-ion batteries. Electrochim Acta 259:566–577

Lai X, Huang Y, Gu H, Han X, Feng X, Dai H, Zheng Y, Ouyang M (2022) Remaining discharge energy estimation for lithium-ion batteries based on future load prediction considering temperature and ageing effects. Energy 238:121754

Lee K-T, Dai M-J, Chuang C-C (2018) Temperature-compensated model for lithium-ion polymer batteries with extended Kalman filter state-of-charge estimation for an implantable charger. IEEE Trans Ind Electron 65(1):589–596

Lin Q, Wang J, Xiong R, Shen W, He H (2019) Towards a smarter battery management system: a critical review on optimal charging methods of lithium ion batteries. Energy 183:220–234

McCollum D, Krey V, Kolp P, Nagai Y, Riahi K (2014) Transport electrification: a key element for energy system transformation and climate stabilization. Clim Change 123(3–4):651–664

Meng J, Ricco M, Luo G, Swierczynski M, Stroe D-I, Stroe A-I, Teodorescu R (2018) An Overview and comparison of online implementable SOC estimation methods for lithium-ion battery. IEEE Trans Ind Appl 54(2):1583–1691

Naslin P (1968) Essentials of optimal control. Illife Books Ltd., London

Pavković D, Sedić A, Guzović Z (2016) Oil drilling rig diesel power-plant fuel efficiency improvement potentials through rule-based generator scheduling and utilization of battery energy storage system. Energy Convers Manag 121:194–211

Pavković D, Krznar M, Komljenović A, Hrgetić M, Zorc D (2017) Dual EKF-based state and parameter estimator for a $LiFePO_4$ battery cell. J Power Electron 17(2):398–410

Pavković D, Komljenović A, Hrgetić M (2013) Control-oriented modeling and experimental identification of a VRLA battery. In: Proceedings of 17th international conference on electrical drives and power electronics (EDPE 2013), Dubrovnik, Croatia. pp 2–9

Pavković D, Lobrović M, Hrgetić M, Komljenović A, Smetko V (2014) Battery current and voltage control system design with charging application. In: Proceedings of 2014 IEEE multi-conference on systems and control, Antibes, France. pp 1133–1138

Pavković D, Komljenović A, Hrgetić M, Krznar M (2015) Experimental characterization and development of a SoC/SoH estimator for a $LiFePO_4$ battery cell. In: Proceedings of IEEE EUROCON 2015, Salamanca, Spain. pp 397–402

Plett GL (2004) Extended Kalman filtering for battery management systems of LiPB-based HEV battery packs – Part 3: state and parameter estimation. J Power Sources 134(2):277–262

Rai R, Gaglani M, Das S, Panigrahi T (2020) Multi-level constant current based fast li-ion battery charging scheme with LMS based online state of charge estimation. In: Proceedings of 2020 IEEE Kansas power and energy conference (KPEC 2020), Manhattan, KS, USA. p 6

Roscher MA, Sauer DU (2011) Dynamic electric behavior and open-circuit-voltage modeling of LiFePO4-based lithium-ion secondary batteries. J Power Sources 196(1):331–336

Samadi MF, Saif M (2017) State-Space modeling and observer design of li-ion batteries using takagi-sugeno fuzzy system. IEEE Trans Control Syst Technol 25(1):301–308

Schröder D (2007) Elektrische antriebe - regelung von antriebssystemen. Springer, Berlin

Scioletti MS, Newman AM, Goodman JK, Zolan AJ, Leyffer S (2017) Optimal design and dispatch of a system of diesel generators, photovoltaics and batteries for remote locations. Optim Eng 18:755–792

Soldo J, Škugor B, Deur J (2021) Analysis of optimal battery state-of-charge trajectory patterns for blended mode of a parallel plug-in hybrid electric vehicle and a wide range of driving conditions. Optim Eng 22:1955–1977

Szumanowski A, Chang Y (2008) Battery management system based on battery nonlinear dynamics modeling. IEEE Trans Veh Technol 57(3):1425–1432

Vo TT, Chen X, Shen W, Kapoor A (2015) New charging strategy for lithium-ion batteries based on the integration of Taguchi method and state of charge estimation. J Power Sources 273:413–422

Wai RJ, Jhung SJ (2012) Design of energy-saving adaptive fast-charging control strategy for Li-Fe-PO_4 battery module. IET Power Electron 5(9):1684–1693

Wang Y, Fang H, Zhou L, Wada T (2017) Revisiting the state-of-charge estimation for lithium-ion batteries: a methodical investigation of the extended Kalman filter approach. IEEE Control Syst Mag 37(4):73–96

Wei Z, Hu J, He H, Li Y, Xiong B (2021) Load current and state-of-charge coestimation for current sensor-free lithium-ion battery. IEEE Trans Power Electron 36(10):10970–10795

Williams BW (1992) Power electronics: devices, drivers, applications and passive components. McGraw-Hill, New York

Wu X, Li X, Du J (2018) State of charge estimation of lithium-ion batteries over wide temperature range using unscented Kalman filter. IEEE Access 6:41993–42003

Xiong R, Cai J, Yu Q, He H, Sun F (2018) Critical review on the battery state of charge estimation methods for electric vehicles. IEEE Access 6:1832–1843

Zhang C, Kang L, Deng J, Song S (2017) Improved realtime state-of-charge estimation of $LiFePO_4$ battery based on a novel thermoelectric model. IEEE Trans Ind Electron 64(1):654–663

Zhang H, Ma J, Zhao X, Zhang D, He Y (2019) State of charge estimation for lithium battery based in adaptively weighting cubature particle filter. IEEE Access 7:166657–166666

Zou C, Hu X, Wei Z, Tang X (2017) Electrothermal dynamics-conscious lithium-ion battery cell-level charging management via state-monitored predictive control. Energy 141:250–259

Zou C, Hu X, Wei Z, Wik T, Egardt B (2018) Electrochemical estimation and control for lithium-ion battery health-aware fast charging. IEEE Trans Industr Electron 65(8):6635–6645